Model of the photon-avalanche effect

M. F. Joubert, S. Guy, and B. Jacquier
Laboratoire de Physico-Chimie des Matériaux Luminescents, Université Claude Bernard Lyon I, Bâtiment 205, 43 boulevard du 11-11-1918, 69622 Villeurbanne CEDEX, France
(Received 5 February 1993)

The photon-avalanche effect, which involves both absorption from a metastable intermediate level and cross-relaxation energy transfer, introduces a new trend in the achievement of efficient up-conversion lasers. In this paper, we report a quite general theoretical treatment of this process which is successfully applied to the case of $LiYF_4:Nd^{3+}$. This model shows clearly that the avalanche effect may occur, above a pumping threshold, only if the cross-relaxation energy-transfer probability is higher than the relaxation rate from the up-converted excited state to the levels located below the metastable intermediate state.

I. INTRODUCTION

Several recent demonstrations of up-conversion-pumped solid-state lasers have renewed the interest in excitation mechanisms that result in emission at a wavelength shorter than that of the pump light. Efficient up-conversion is possible in rare-earth-doped materials with metastable, intermediate levels that can act as a storage reservoir for pump energy. The rare-earth-doped solid-state up-conversion lasers mentioned in the literature were pumped via excited-state absorption[1–8] or energy-transfer processes.[9–18] These up-conversion lasers are tabulated in Table I with their pump wavelength, emission wavelength, operating temperature, and approximate overall efficiency. In this table, it appears clearly that the $LiYF_4:Nd^{3+}$,[3,4] $LaCl_3:Pr^{3+}$,[6] and $LiYF_4:Tm^{3+}$ (Refs. 7 and 8) laser systems, which are pumped by an avalanche mechanism, belong to the most efficient up-conversion laser systems. So, the investigation of this process seems to be necessary to get a better knowledge of the mechanism and find good candidates as solid-state up-conversion lasers which may operate at room temperature.

The phenomenon of photon avalanche was first discovered in Pr^{3+}-based infrared quantum counters.[19] A $LaCl_3$ or $LaBr_3$ crystal doped with Pr^{3+} was exposed to laser-pump radiation, in which the frequency matches the excited-state transition absorption $^3H_5 \Longrightarrow {}^3P_1$. When this radiation was slightly in excess of a certain critical intensity, Pr^{3+} fluorescence increases by orders of magnitude and, correspondingly, pump absorption was sufficient to cause a dimming of the laser light on passing through the crystal. This phenomenon was due to an efficient cross-relaxation energy transfer between the lowest infrared levels of Pr^{3+} which induces the excited-state absorption used in the quantum counter process. Such an avalanche process was also observed with other rare-earth-doped crystals such as $LaBr_3:Sm^{3+}$,[20] $LiYF_4:Nd^{3+}$,[3,4] $LaCl_3:Pr^{3+}$,[6] $LiYF_4:Tm^{3+}$,[7,8] and $YAlO_3:Tm^{3+}$.[21]

The main goal of this paper is to study the avalanche process from a theoretical point of view and to apply the theory to the experimental results obtained in the case of $LiYF_4:Nd^{3+}$. Section II is devoted to the theory of cross-relaxation-induced excited-state absorption and to the critical parameters leading to the possibility for the avalanche to be observed. Section III describes crystallographic and optical properties of $LiYF_4:Nd^{3+}$ as well as the experimental equipment used in this study. The experimental results are presented in Sec. IV and their interpretation is given in Sec. V. Finally, some conclusions are drawn in Sec. VI.

II. THEORY

The avalanche phenomenon may occur in the case where an efficient cross-relaxation energy-transfer induces an excited-state absorption mechanism. Nevertheless, this is not a sufficient condition for the avalanche to

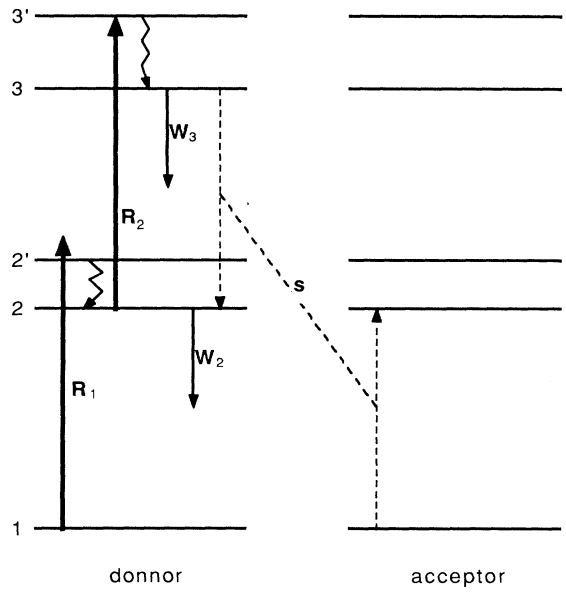

FIG. 1. General energy scheme for an avalanche process.

happen. The theoretical development which follows will permit us to determine the necessary and sufficient conditions to observe an avalanche.

Figure 1 shows the general energy scheme for an avalanche process. The nonresonant absorption from the ground state populates the level 2′, which relaxes nonradiatively to the metastable level 2. The resonant absorption $2 \Longrightarrow 3'$, followed by the nonradiative relaxation $3' \Longrightarrow 3$, leads to the population of the emitting level 3. Then the cross-relaxation process, noted by the dotted arrows in Fig. 1, permits a very efficient population of level 2 and enhances the excited-state absorption $2 \Longrightarrow 3'$. Since the phonon relaxations are fast compared to all other processes involved, the excitation process can be adequately described by the following rate equations where n_1, n_2, and n_3 denote the populations in level 1, 2, and 3, respectively:

$$\begin{aligned}
\frac{dn_1}{dt} &= -R_1 n_1 + W_2 n_2 + b W_3 n_3 - s n_1 n_3 \ , \\
\frac{dn_2}{dt} &= R_1 n_1 - (W_2 + R_2) n_2 + (1-b) W_3 n_3 + 2 s n_1 n_3 \ , \qquad (1) \\
\frac{dn_3}{dt} &= R_2 n_2 - W_3 n_3 - s n_1 n_3 \ ,
\end{aligned}$$

with

$$n_1 + n_2 + n_3 = 1 \ .$$

The nonresonant absorption from the ground-state and the resonant excited-state absorption are characterized by pumping rates R_1 and R_2, respectively. W_2 and W_3 are the relaxation rates of levels 2 and 3, respectively. The branching in the decay of level 3 is described by the parameter b with $(1-b)W_3$ being the decay rate to level 2. The energy-transfer process that couples the Nd^{3+} ions is described by the parameter s.

A. Stationary solutions

The system (1) can be solved explicitly in the long-time limit. The stationary solution for the level 3 population is

$$n_3^{\infty} = \frac{B}{2A} \left[-1 + \mathrm{sgn}(B) \left[1 + \frac{4AR_1}{B^2} \right]^{1/2} \right] , \qquad (2)$$

with

TABLE I. Examples of rare-earth-doped solid-state up-conversion lasers.

Ion	Host	Laser emission wavelength (nm)	Pump wavelength (nm)	Mechanism	Temperature (K)	Overall efficiency	Reference
Er^{3+}/Yb^{3+}	BaY_2F_8	670	ir flash lamp	energy transfer	77		9
Ho^{3+}/Yb^{3+}	BaY_2F_8	551.5	ir flash lamp	energy transfer	77		9
Er^{3+}	$YAlO_3$	550	792.1+839.8	sequential two-photon absorption	$T \leq 77$	≈0.4% at 30 K	1
Er^{3+}	$BaYb_2F_8$	670	1045	energy transfer	room temperature		10
Er^{3+}	$LiYF_4$	551	797 or diode 791	energy transfer plus sequential two-photon absorption	$T \leq 90$	0.2% at 40 K	11,12
Nd^{3+}	LaF_3	380	788+591	sequential two-photon absorption	$T \leq 90$	3% at 20 K	2
		730	603.6	avalanche	$T \leq 40$	11% at 12 K	3,4
Nd^{3+}	$LiYF_4$	413	603.6	avalanche	$T \leq 40$	4.3% at 12 K	3,4
Tm^{3+}	$LiYF_4$	450.2	781+647.9 pulsed lasers	sequential two-photon absorption	room temperature	1.3%	5
Pr^{3+}	$LaCl_3$	644	677	avalanche 80 ⟹ 300 K	$80 < T < 210$	25% at 80 K	6
Er^{3+}	CaF_2	855	1510	cooperative transfer	77	17.8%	13
		469.7	969.3	energy transfer	$T \leq 35$	0.3%	14
		469.7	653.2	energy transfer	$T \leq 35$	4.6%	14
Er^{3+}	$LiYF_4$	560.6	969.3	energy transfer	$T \leq 35$	2%	14
Tm^{3+}	$LiYF_4$	450.2	784.5+648	sequential two-photon absorption	$T \leq 70$	2% at 15 K	7,8
Tm^{3+}	$LiYF_4$	483	628	avalanche	$T \leq 130$	7.5% at 26 K	7,8
Tm^{3+}	$LiYF_4$	483	647.9	avalanche	$T \leq 160$		8
Tm^{3+}/Yb^{3+}	BaY_2F_8	455,510,649, 799	960	energy transfer	room temperature		15
Er^{3+}	$LiYF_4$	551	1550	cooperative transfer	$T \leq 95$	≈7.5% at 9 K	16
Er^{3+}	$LiYF_4$	467	1550	cooperative transfer	70		17
		470,554,555	792.4	cooperative transfer	10		18
		552	792.4	cooperative transfer	40		18
Er^{3+}	BaY_2F_8	617,669	792.4	cooperative transfer	20		18

$$A=\frac{s}{R_2}[R_2+W_3(1+b)-W_2]\ ,$$

$$B=\frac{1}{R_2}[W_2(W_3+s)-R_2(s-bW_3)+R_1W_3+R_1R_2]\ .$$

As we mentioned before, R_1 is the pumping rate from the ground state which corresponds to a nonresonant absorption. Thus we may assume that R_1 is very small compared to all the other terms. So

$$\left[1+\frac{4AR_1}{B^2}\right]^{1/2}\approx 1+\frac{2AR_1}{B^2}\ .$$

This leads to the following solutions for n_3^∞: if $B>0$,

$$n_3^\infty=\frac{R_1R_2}{W_2(W_3+s)-R_2(s-bW_3)+R_1R_2+R_1W_3}$$

$$\approx\frac{R_1R_2}{s-bW_3}\frac{1}{R_{2\,\text{limit}}-R_2}\ , \tag{3}$$

and if $B<0$,

$$n_3^\infty=\frac{-W_2(W_3+s)+R_2(s-bW_3)-R_1R_2-R_1W_3}{s[W_3(1+b)+R_2-W_2]}$$

$$\approx(s-bW_3)\frac{R_2-R_{2\,\text{limit}}}{s[W_3(1+b)+R_2-W_2]}, \tag{4}$$

where

$$R_{2\,\text{limit}}=\frac{W_2(s+W_3)}{s-bW_3}\ . \tag{5}$$

Note that

$$B<0\Longleftrightarrow R_2>R_{2\,\text{limit}}\ ,$$

$$B>0\Longleftrightarrow R_2<R_{2\,\text{limit}}\ .$$

If $s<bW_3$, $B>0$. So, only the first regime exists, whatever the excitation power is. On the other hand, if $s>bW_3$, the two regimes exist. Above the threshold ($R_2=R_{2\,\text{limit}}$), there is the avalanche effect. In conclusion, the avalanche effect may occur only if the cross-relaxation probability (s) is higher than the relaxation probability from level 3 to level 1 (bW_3).

B. General solution under low excitation density

In the system (1), the analytical expression of $n_3(t)$ cannot be found explicitly in the general case. Nevertheless, for low excitation densities, it is reasonable to assume that $n_1\approx 1$. So, if we do the variable change

$$n_1=1-a_1\ ,$$

n_2, n_3, and a_1 are very small compared to 1. Then, we may neglect the term sa_1n_3 in the first order. The system (1) is then reduced to the following linear system:

$$\frac{dn_2}{dt}=-\alpha n_2+\beta n_3+R_1\ ,$$

$$\frac{dn_3}{dt}=R_2n_2-\gamma n_3\ , \tag{6}$$

$$a_1=n_2+n_3\ ,$$

with

$$\alpha=R_2+R_1+W_2,\quad \beta=(1-b)W_3+2s-R_1,$$

$$\gamma=W_3+s\ .$$

As we mentioned before, R_1 is the pumping rate from the ground state which corresponds to a nonresonant absorption. Thus we may assume that R_1 is very small compared to the other terms. This leads to

$$\alpha\approx R_2+W_2,\quad \beta\approx(1-b)W_3+2s\ .$$

The analytical solution of the system (6) is

$$n_3(t)=[1+(C-0.5)^{-(D+E)t}-(C+0.5)e^{-(D-E)t}]n_3^\infty \tag{7}$$

with

$$D=0.5(\alpha+\gamma)\ ,$$

$$E=0.5\sqrt{(\alpha-\gamma)^2+4R_2\beta}\ ,$$

$$C=\frac{E\gamma}{2R_2\beta}+\frac{\alpha-\gamma}{4E}-\frac{\gamma(\alpha-\gamma)^2}{8R_2\beta E}=\frac{\alpha+\gamma}{4E}\ ,$$

$$n_3^\infty=\frac{R_1R_2}{W_2(W_3+s)-R_2(s-bW_3)+R_1R_2+R_1W_3}+R_1s.$$

Equation (7) is a good solution as soon as the coefficients in the exponential part are negatives, so $n_3(t)$ does not diverge. This leads to stable solutions only if

$$s<bW_3\ \text{ or }\ s>bW_3\ ,\quad R_2<R_{2\,\text{limit}}=\frac{W_2(s+W_3)}{s-bW_3}\ .$$

In other words, this analytical solution for $n_3(t)$ is valid only below the avalanche threshold.

C. Numerical approach

As, in the system (1), the analytical expression of $n_3(t)$ cannot be found explicitly in the high excitation density regime, we have to solve numerically the equations. A numerical resolution of the time evolution of the transmission using the formula

$$T=1-(R_1n_1+R_2n_2)\frac{dl}{I}\frac{hc}{\lambda}\ , \tag{8}$$

where d is the Nd^{3+} concentration, l is the sample thickness, and I is the pump intensity, may be done also.

III. MATERIAL AND EXPERIMENTAL EQUIPMENT

Such an avalanche process was recently observed in the case of $LiYF_4$:1 at. % Nd^{3+}, which is a relatively efficient up-conversion laser at low temperature[3,4] and the energy-level diagram describing the process is presented in Fig. 4 of Ref. 4. The excitation laser frequency was in resonance with the excited-state absorption transition between the lower Stark components of the $^4F_{3/2}$ and $^4D_{3/2}$ manifolds and the anti-Stokes lasing transitions come from deexcitation of the $^2P_{3/2}$ level. In this work, we recorded the power dependence of the laser intensity

transmitted by the sample and of the anti-Stokes emission intensity in this material to try to get a better knowledge of the parameters involved in this phenomenon.

A. Material

The lithium yttrium fluoride has the quadratic scheelite structure. The sample used in this study is an optically polished thin plate of $5\times1.73\times1.29$ mm^3, the c crystallographic direction being parallel to the higher dimension. The excited-state absorption transition between the lower Stark components of the $^4F_{3/2}$ and $^4D_{3/2}$ manifolds has no preferential polarization. For our measurements, the crystallographic c axis was transverse to the laser axis as in previous work.[3]

B. Experimental equipment

The experimental setup is presented in Fig. 2. The sample is placed in a liquid-helium optical cryostat with a heating gas system and a regulator device allowing the temperature to be varied between 1.6 and 300 K. Laser excitation was achieved by a Spectra Physics model 380 ring dye laser pumped by a cw Coherent 10-W argon laser. The wavelength of the excitation laser beam was fixed at 6036 Å, which is the wavelength of the excited-state absorption transition between the lower Stark components of the $^4F_{3/2}$ and $^4D_{3/2}$ manifolds. The laser beam was chopped and focused on the sample. The violet anti-Stokes emission related to the $^2P_{3/2}\Longrightarrow{}^4I_{11/2}$ was collected at 90° to the laser beam direction and analyzed

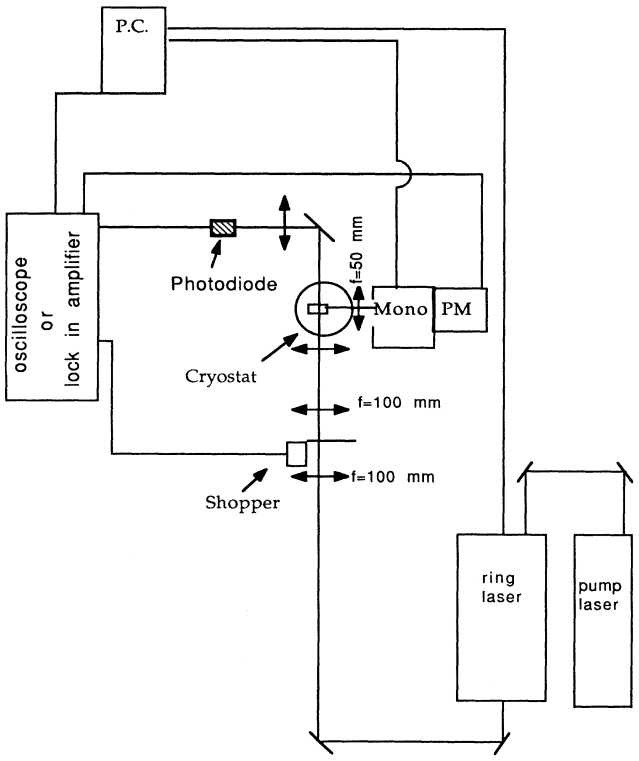

FIG. 2. Experimental setup.

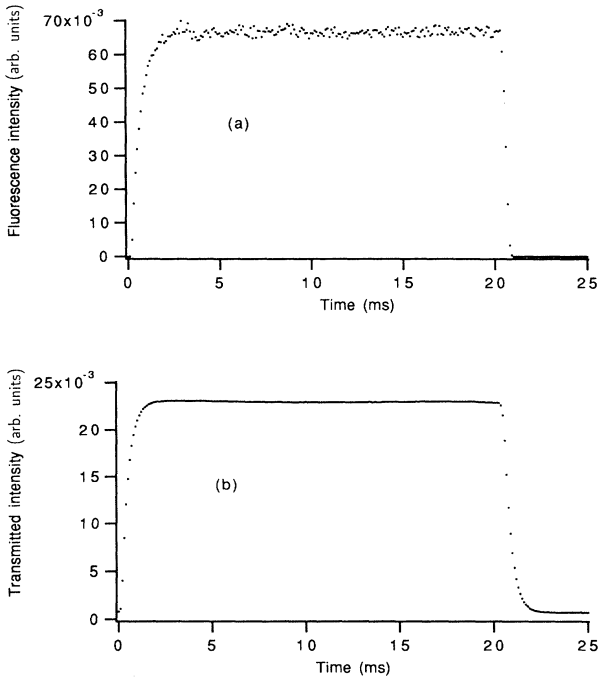

FIG. 3. Experimental anti-Stokes (a) fluorescence (4130 Å) and (b) transmission intensity versus time during laser (6036 Å) illumination at 165 K with an excitation power of 110 mW and a 80-mm focal lens.

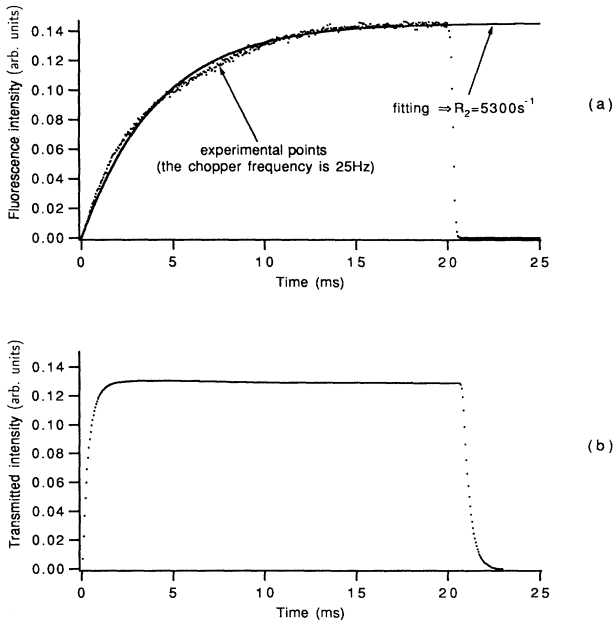

FIG. 4. Experimental anti-Stokes (a) fluorescence (4130 Å) intensity and (b) transmission intensity versus time during laser (6036 Å) illumination at 6 K with an excitation power of 110 mW and a 80-mm focal lens.

by a 1/4-m Jarrel Ash monochromator followed by a EMI 9789QB photomultiplier. Simultaneously, the laser intensity transmitted through the sample was sent to a photodiode. These two signals were analyzed by a LeCroy 9410 digital oscilloscope or to a lock-in amplifier. This experimental setup was controlled by a personal computer.

IV. EXPERIMENTAL RESULTS

The first study was to record the time evolution of the transmitted laser light intensity and of the violet anti-Stokes emission intensity during the illumination of the sample. The laser beam was fixed at 6036 Å. The selected anti-Stokes fluorescence was the intense $^2P_{3/2} \Longrightarrow {}^4I_{11/2}$ line located at 4130 Å, which is known to be a very efficient laser emission after up-conversion pumping.[3] Figure 3 shows the experimental result obtained at 165 K using an excitation power of 110 mW focused on the sample with a 80-mm lens. The transmitted laser light as well as the violet fluorescence are constant. At liquid-

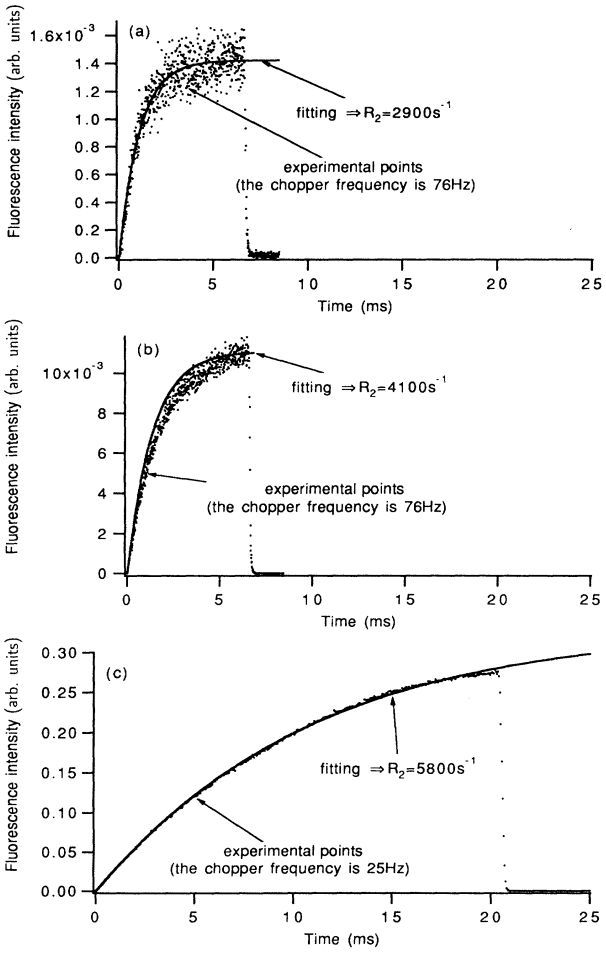

FIG. 5. Experimental anti-Stokes fluorescence (4130 Å) intensity versus time during laser (6036 Å) illumination at 6 K for different excitation density: (a) 13 mW and a 80-mm focal lens, (b) 22 mW and a 80-mm focal lens, and (c) 115 mW and a 50-mm focal lens.

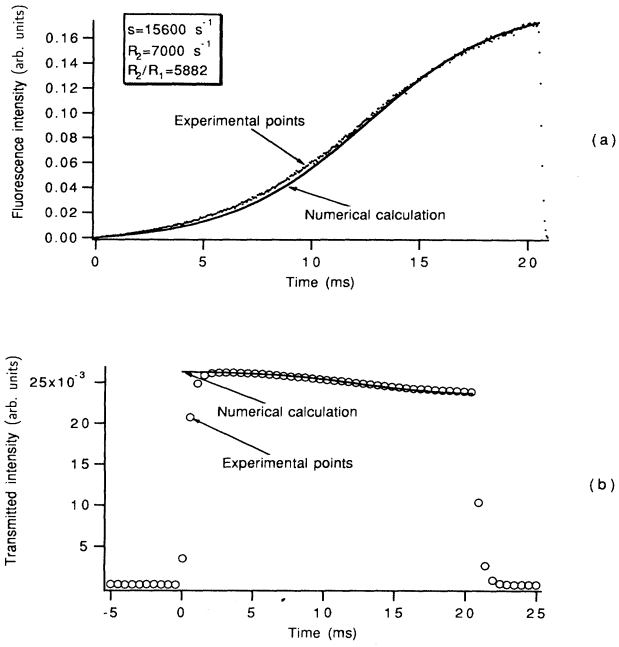

FIG. 6. Experimental anti-Stokes (a) fluorescence (4130 Å) and (b) transmission intensity versus time during laser (6036 Å) illumination at 6 K with an excitation power of 160 mW and a 50-mm focal lens.

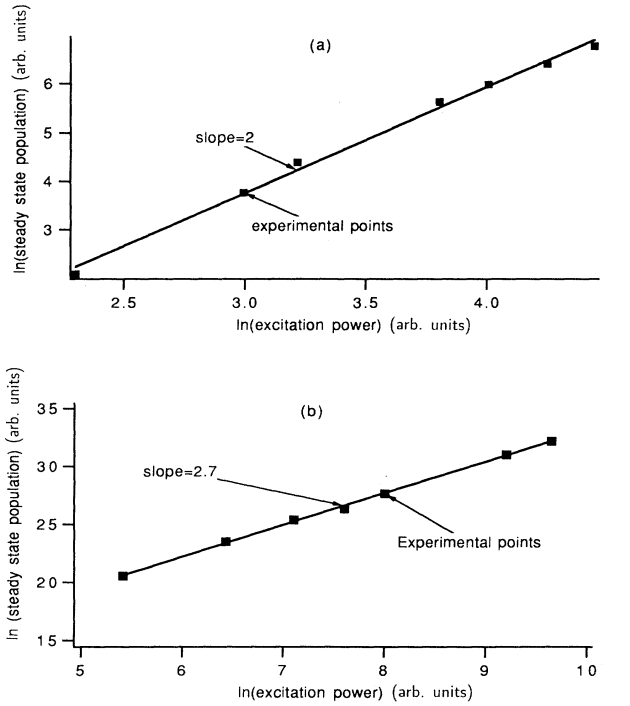

FIG. 7. Logarithm of the experimental anti-Stokes fluorescence (4130 Å) intensity versus the logarithm of the excitation laser (6036 Å) power (a) at very low excitation densities and (b) at higher excitation densities.

helium temperature, the experimental result is quite different concerning the anti-Stokes emission time dependence. Indeed, Fig. 4 shows that, for the same excitation condition, the anti-Stokes fluorescence shows a rise time over about 15 ms, and then it becomes constant. We looked at the excitation density evolution of this rise time either by using lower laser power [Figs. 5(a) and 5(b)] or, to get higher excitation density, by using a shorter focal lens [Fig. 5(c)]. It is clear that this rise time increases with the excitation density. Finally, at very high excitation density (160-mW focused with the 50-mm lens), the violet emission becomes extremely intense and the experimental curves presented in Fig. 6 show that now, the establishment of the violet anti-Stokes fluorescence is quite long and presents a bending point; in the same way, the transmitted laser light decreases of about 12%. This behavior is characteristic of an avalanche process.

We also recorded the power dependence of the violet anti-Stokes fluorescence line at 4130 Å. The result is presented in Fig. 7. The logarithmic plot shows first [Fig. 7(a)] a quadratic behavior and then [Fig. 7(b)] a slope of 2.7.

V. INTERPRETATION

Now, we want to apply the theory developed in Sec. II to the $LiYF_4:Nd^{3+}$ case. The energy levels 1, 2, 2′, 3, and 3′ mentioned in the theoretical treatment are related to the $^4I_{9/2}$, $^4F_{3/2}$, $^2H_{11/2}$, $^2P_{3/2}$, and $^4D_{3/2}$ Nd^{3+} manifolds. The measured values of the relaxation rates W_2 and W_3 are, respectively, 1905 and 20 000 s^{-1}.[3]

A. Below the avalanche threshold

The experimental results presented in Figs. 4 and 5, relative to the $^2P_{3/2}$ population $n_3(t)$, may be fitted using Eq. (7), which is valid only below the avalanche threshold. The three parameters are the branching ratio b and the cross relaxation transfer probability s, which are constant, and the pumping rate R_2, which increases with the excitation power. The best fits presented in Figs. 4 and 5 are obtained with $b=0.2$, $s=15\,600$ s^{-1}, and $R_2=2900$, 4100, 5300, and 5800 s^{-1}. It appears that the cross-relaxation transfer probability s is larger than $bW_3=4000$ s^{-1}. According to the theory, that means that an avalanche is possible above the threshold value $R_{2\,\mathrm{limit}}=5846$ s^{-1}.

B. Above the avalanche threshold

Above the threshold, the only way to make a theoretical approach is to solve numerically the system (1). Figure 6(a) shows the result of modeling calculation using the parameters $b=0.2$, $s=15\,600$ s^{-1}, $R_2=7000$ s^{-1}, and $R_2/R_1=5882$. This resolution is quite satisfactory as it shows that now R_2 is larger than $R_{2\,\mathrm{limit}}=5846$ s^{-1}. Moreover, the value of R_2/R_1 is high as it was assumed in Sec. II.

Figure 6(b) shows the result of modeling calculation for the transmission using the same parameters. The agreement between the experimental and calculated curves is perfect for an incident power $I=73$ kW/cm^2. This permitted us to estimate the excited-state absorption cross section using the well-known formula

$$\sigma=\frac{\hbar\omega R_2}{I}\ .$$

We found $\sigma=3.2\times10^{-20}$ cm^2. Using the Judd-Ofelt parameters of Nd^{3+} in this host calculated recently,[22] this cross section may be approximately evaluated to 2×10^{-20} cm^2 at room temperature. This value is not exactly comparable to the previous one, which was estimated using the avalanche experimental results at liquid-helium temperature. Nevertheless, these two values are in the same order of magnitude, which is quite satisfactory.

C. Stationary solutions

Using Eqs. (3) and (4), the calculated power dependence of the $^2P_{3/2}$ population is drawn in Fig. 8. It is in perfect agreement with the experimental results as it shows that, for values of R_2 higher than ~5850 s^{-1}, n_3^∞ becomes much higher. Below this threshold, the logarithmic plot of Fig. 8 indicated a quadratic behavior at very low pumping rate ($R_2<1000$ s^{-1}) and then a slope of 2.6 as it was observed experimentally (see Fig. 7).

VI. CONCLUSION

In this study, we tried to make a complete treatment of the avalanche process from a theoretical and experimental point of view. Such a phenomenon may occur in the case where an efficient cross-relaxation energy transfer induces an excited-state absorption mechanism. The main condition for a cross-relaxation energy transfer to be efficient is the perfect coincidence between the energy gaps involved in the process. Nevertheless, this condition is not sufficient for the avalanche to happen. The theoretical model shows clearly that the avalanche effect may occur only if the probability of the cross-relaxation energy transfer involved in the process is higher than the relaxation probability from level 3 to level 1 (see Fig. 1).

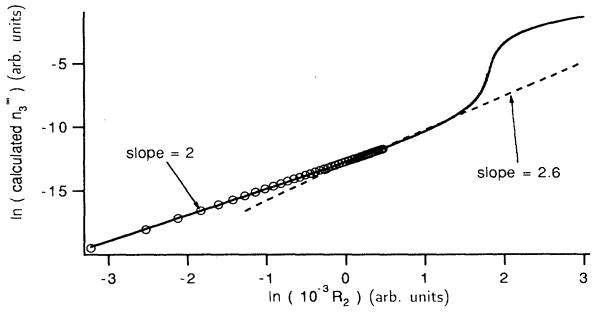

FIG. 8. Logarithm of the calculated anti-Stokes fluorescence (4130 Å) intensity versus the logarithm of the pumping rate R_2. The dotted line and the marker line are theoretical fittings with a linear function.

Indeed, such a condition is satisfied in $LiYF_4$:1 at. % Nd^{3+}, as probed by the theoretical treatment of the avalanche experimental data. This is great progress for the prediction of new materials giving rise to an efficient up-conversion of pump light. The model developed in this article may be used to interpret the avalanche process whatever the material is. Now, we plan to extend this theory to the case where two different kinds of ion are involved in the process.

ACKNOWLEDGMENTS

We thank R. M. Macfarlane of the Almaden Research Center, IBM, for providing us with the single crystal used in this study and for helpful discussions. We also acknowledge C. Linarès of our laboratory for helping us in the cross-section Judd-Ofelt calculation. Laboratoire de Physico-Chimie des Matériaux Luminescents is Unité de Recherche Associée au CNRS No. 442.

[1]A. J. Silversmith, W. Lenth, and R. M. Macfarlane, J. Opt. Soc. Am. A **3**, 128 (1986); Appl. Phys. Lett. **51**, 1977 (1987).

[2]R. M. Macfarlane *et al.*, Appl. Phys. Lett. **52**, 1300 (1988).

[3]F. Tong, R. M. Macfarlane, and W. Lenth (unpublished).

[4]W. Lenth and R. M. Macfarlane, J. Lumin. **45**, 346 (1990).

[5]D. C. Nguyen *et al.*, Appl. Opt. **28**, 3553 (1989); SPIE J. **1223**, 54 (1990).

[6]M. E. Koch, A. W. Kueny, and W. E. Case, Appl. Phys. Lett. **56**, 1083 (1990).

[7]R. M. Macfarlane, R. Wannemacher, T. Hebert, and W. Lenth, in *Conference on Lasers and Electro-Optics, 1990 Technical Digest Series, Vol. 7* (Optical Society of America, Washington, D.C., 1990), p. 250.

[8]T. Hebert, R. Wannemacher, R. M. Macfarlane, and W. Lenth, Appl. Phys. Lett. **60**, 2592 (1992).

[9]L. F. Johnson and G. J. Guggenheim, Appl. Phys. Lett. **19**, 44 (1971).

[10]B. M. Antipenko *et al.*, Zh. Tekh. Fiz. **57**, 349 (1987) [Sov. Phys.–Tech. Phys. **32**, 208 (1987)].

[11]W. Lenth *et al.*, *Advances in Laser Science* III, edited by A. C. Tam, J. L. Gole, and W. C. Stwalley, AIP Conf. Proc. No. 172 (AIP, New York, 1987), p. 8; F. Tong, W. P. Risk, R. M. Macfarlane, and W. Lenth, Electron. Lett. **25**, 1389 (1989), R. A. McFarlane, Appl. Phys. Lett. **54**, 2301 (1989).

[12]G. C. Valley and R. A. McFarlane, in *OSA Proceedings on Advanced Solid-State Lasers,* edited by Lloyd L. Chase and Albert A. Pinto (Optical Society of America, Washington, D.C., 1992), Vol. 13, pp. 376–379.

[13]P. Xie and S. C. Rand, Appl. Phys. Lett. **57**, 1182 (1990).

[14]T. Hebert, R. Wannemacher, W. Lenth, and R. M. Macfarlane, Appl. Phys. Lett. **57**, 1727 (1990).

[15]R. J. Thrash and L. F. Johnson (unpublished).

[16]P. Xie and S. C. Rand, Opt. Lett. **17**, 1198 (1992).

[17]R. M. Macfarlane (private communication).

[18]R. A. McFarlane, in *OSA Proceedings on Advanced Solid-State Lasers* (Ref. 12), pp. 275–279.

[19]J. S. Chivian, W. E. Case, and D. D. Eden, Appl. Phys. Lett. **35**, 124 (1979); A. W. Kueny, W. E. Case, and M. E. Koch, J. Opt. Soc. Am. **6**, 639 (1989); W. E. Case, M. E. Koch, and A. W. Kueny, J. Lumin. **45**, 351 (1990).

[20]N. J. Krasutsky, J. Appl. Phys. **54**, 1261 (1983).

[21]H. Ni and S. C. Rand, Opt. Lett. **16**, 1424 (1991).

[22]C. Li, Y. Guyot, C. Linarès, R. Moncorgé, and M. F. Joubert, *Advanced Solid-State Lasers and Compact Blue-Green Lasers, Technical Digest, 1993* (Optical Society of America, Washington, D.C., 1993), Vol. 2, pp. 423–425.